

Rotary Ultrasonic Motors Actuated By Traveling Flexural Waves

Yoseph Bar-Cohen^a, Xiaoqi Bao^a, and Willem Grandia^b,

^aJet Propulsion Laboratory, Caltech, Pasadena, CA 91109, yosi@jpl.nasa.gov

^bQuality Material Inspection (QMI), Costa Mesa, CA 92627

ABSTRACT

Efficient miniature actuators that are compact and consume low power are needed to drive space and planetary mechanisms in future NASA missions. Ultrasonic rotary motors have the potential to meet this NASA need and they are developed as actuators for miniature telerobotic applications. These motors have emerged in commercial products but they need to be adapted for operation at the harsh space environments that include cryogenic temperatures and vacuum and also require effective analytical tools for the design of efficient motors. A finite element analytical model was developed to examine the excitation of flexural plate wave traveling in a piezoelectrically actuated rotary motor. The model uses 3D finite element and equivalent circuit models that are applied to predict the excitation frequency and modal response of the stator. This model incorporates the details of the stator including the teeth, piezoelectric ceramic, geometry, bonding layer, etc. The theoretical predictions were corroborated experimentally for the stator. In parallel, efforts have been made to determine the thermal and vacuum performance of these motors. Experiments have shown that the motor can sustain at least 230 temperature cycles from 0°C to -90°C at 7 Torr pressure significant performance change. Also, in an earlier study the motor lasted over 334 hours at -150°C and vacuum. To explore telerobotic applications for USMs a robotic arm was constructed with such motors.

Keywords: Piezoelectric Motors, Ultrasonic Motors (USMs), Stators and Rotors, Modal Analysis, Actuators, Active Materials

1. INTRODUCTION

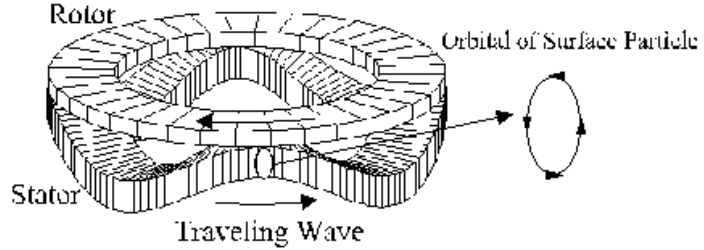
Actuators are used to operate NASA telerobotic devices that include robotic arms and rovers, as well as space mechanism and instruments such as release mechanisms, antenna and instrument deployment, positioners, aperture opening and closing devices. Increasingly, efforts are made to seek actuators that are compact, lightweight and miser. These constraints are necessary to allow meeting growing mission requirements with as many experiments and tasks as possible while conforming to strict mass, size, power, and cost allocations. This trend is straining the specifications of actuation and articulation mechanisms that drive space and planetary instruments. The miniaturization of conventional electromagnetic motors is limited by practical manufacturing difficulties. These types of motors are compromising speed for torque using speed-reducing gears. The use of gear adds mass, volume and complexity as well as decreases the motor drive system reliability due the involvement of a larger number of system components. The recent introduction of rotary ultrasonic motors (USMs) enabled a new effective actuator for drive mechanisms of miniature instruments [Hollerbach, et al 1991, Flynn, 1992, E. Inaba, et al, 1995, and Wallashek, 1995]. These motors have high torque density at low speed, high holding torque, simple construction, and have a quick response. JPL is developing these motors for operation at such planetary environments as Mars over an extended period, where the temperature is as low as -120° C and cyclically changing over range of many tens of degrees between day and night while the ambient pressure is about 6-torr. This range of temperatures and pressures is beyond the specifications of commercial piezoelectric motors even though there is no technical reason why these motors would not work. An alternative stator drive approach was developed to enhance the longevity and planetary operability of these motors. A theoretical model was developed to allow predicting the response of the stator to various drive frequencies and the results were corroborated experimentally.

Generally, ultrasonic motors [Wallashek, 1995] can be classified by their mode of operation (static or resonant), type of motion (rotary or linear) and shape of implementation (beam, rod, disk, etc.). Despite the distinctions, the fundamental principles of solid-state actuation tie them together: microscopic material deformations (usually associated with piezoelectric materials) are amplified through either quasi-static mechanical or dynamic/resonant means. Several of the motor classes have seen commercial application in areas needing compact, efficient, and intermittent motion. Such

applications include: camera auto-focus lenses, watch motors and compact paper handling. Obtaining the levels of torque-speed characteristics of USMs using conventional motors requires adding a gear system to reduce the speed, thus increasing the size, mass and complexity of the drive mechanism. USMs are fundamentally designed to have a high holding force, providing effectively zero backlash. Further, since these motors are driven by friction the torque that would cause them to be backdriven at zero power is significantly higher than the stall torque. The number of components needed to construct ultrasonic motor is small minimizing the number of potential failure points. The general characteristic of USMs makes them attractive for robotic applications where small, intermittent motions are required.

In Figure 1 the principle of operation of an ultrasonic motor (flexural traveling wave ring-type motor) is shown as an example. A traveling wave is established over the stator surface, which behaves as an elastic ring, and produces elliptical motion at the interface with the rotor. This elliptical motion of the contact surface propels the rotor and the drive-shaft connected to it. Teeth on the top section of the stator are intended to form a moment arm to amplify the speed. The operation of USM depends on friction at the interface between the moving rotor and stator, which is a key issue in the design of this interface for extended lifetime.

Figure 1: Principle of operation of a rotary flexural traveling wave motor.



2. MODELING OF STATORS

A stator substrate is assumed to have a thickness, t_s , with a set of piezoelectric crystals that are bonded to the back surface of the stator in a given pattern of poling sequence and location. The thickness of the piezoelectric crystals is t_p . The total height, h , is the sum of the thickness of the crystals and the stators. The overall height of the stator is also allowed to vary with radial position. The outer radius of the disk is b and its inner radius (the hole radius) is a . To generate traveling wave, the poling direction of the piezoelectric crystals is structured such that a quarter wavelength out-of-phase is formed. This poling pattern is also intended to eliminate extension in the stator and maximize bending. The teeth on the stator are arranged in a ring at the radial position. To generate a traveling wave within the stator two orthogonal modes are activated simultaneously. These modes are induced by a stator that is constructed with the drive piezoelectric actuators in the form of two sections of poling pattern that are bonded to the stator. Geometrical examination of this pattern shows that driving the two sections using $\cos(\omega t)$ and $\sin(\omega t)$ signals, respectively, will produce a traveling wave with a frequency of $\omega/2\pi$. Also, by changing the sign on one of the drive signals, the traveling wave would reverse its direction.

2.1 Equations

The equation of motion of an elastic structure including piezoelectric elements can be derived from Hamilton's principle. The finite element model for piezoelectric vibration has been derived by many authors (e.g. Allik et al, Kagawa et al). The discretized equation of the stator can be expressed as

$$\begin{aligned} [M]\{\ddot{\mathbf{x}}\} + [C]\{\dot{\mathbf{x}}\} + [K]\{\mathbf{x}\} &= [P]\{\mathbf{j}\} + \{F\} \\ [P]^T\{\mathbf{x}\} - [G]\{\mathbf{j}\} &= \{Q\} \end{aligned} \quad (1)$$

where $[M]$, $[C]$, $[K]$, $[P]$, $[G]$, are the mass, damping, stiffness, electromechanical coupling, and capacitance matrices, respectively. The vectors $\{\xi\}$, $\{\varphi\}$, $\{F\}$, and $\{Q\}$ are the nodal displacement, the electric potential vectors the normal external force, the tangential external force and the charge vectors, respectively. For simple harmonic motion, we have

$$\begin{aligned} ([K] + j\omega[C] - \omega^2[M])\{\mathbf{x}\} - [P]\{\mathbf{j}\} &= \{F\} \\ [P]^T\{\mathbf{x}\} - [G]\{\mathbf{j}\} &= \{Q\} \end{aligned} \quad (2)$$

The charge at all nodes (not on the electrodes) is zero and the electric potentials at the nodes on the same electrode are equal to each other. Therefore, we have constraints as

$$\begin{aligned} q_1 = q_2 = \dots = 0 & \quad \text{for nodes not on electrodes} \\ \mathbf{j}_1 = \mathbf{j}_2 = \dots = V_e & \quad \text{for nodes on electrodes} \end{aligned} \quad (3)$$

where V_e is the voltage on electrode e .

2.2 The 3D Model Analysis for the Stator

The structure of the stator that we modeled is presented in Figure 2, which includes PZT ring, bonding layer and a metal disk with varied cross section and teeth. The electrodes of the PZT ring are patterned to excite 5-wave mode vibration of the stator.

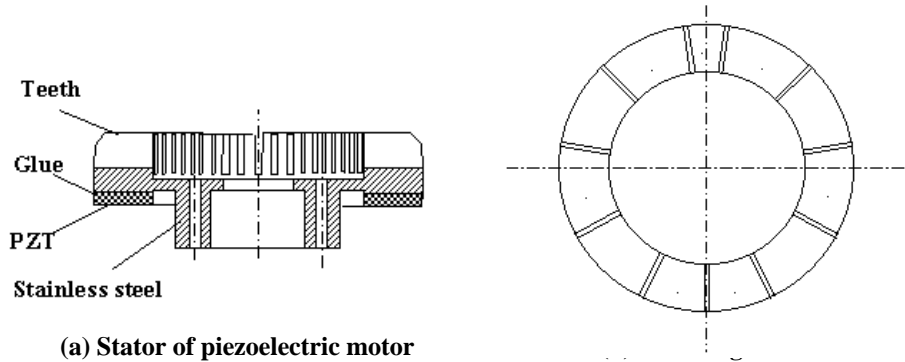
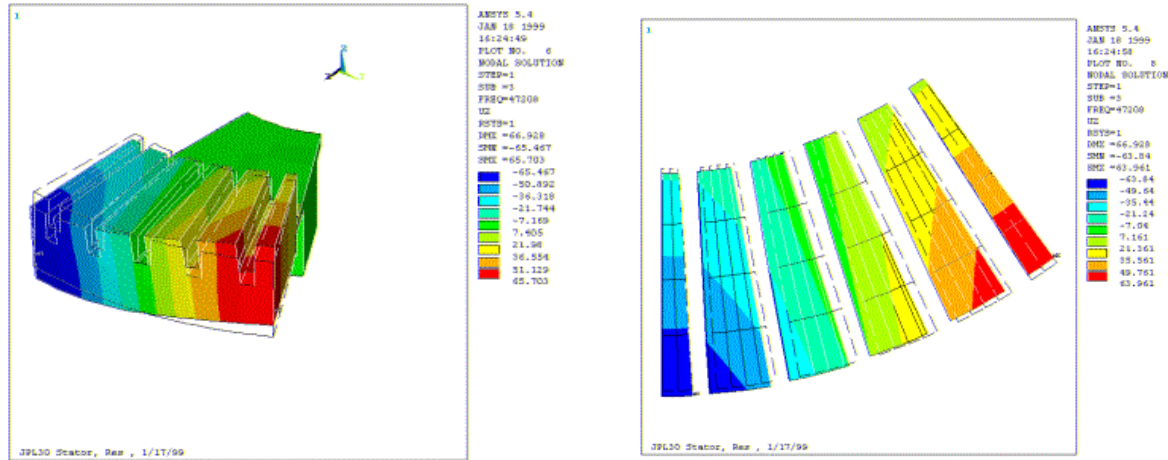


Figure 2: Piezoelectric stator and PZT ring

The modal analysis is used to analyze the resonance of the stator, determine the resonance frequencies and model shapes by assigning zero to $[C]$, $\{F\}$ and all V_e and solving the eigenvalue problem of Eq. (2) with constraint (3).



(a) 45° view

(b) Top view of teeth

Figure 3: The modal shape for 1/2 wavelength sector

This 3D finite element model enables the simulation of complex structures and to obtain more accurate results than other approaches e.g. analytical models or annual finite element models. However, the computational process is time consuming and far from being practical when using a personal computers or workstations to determine the full model of the stator with finer meshes. Using the symmetry of the stator structure, a fraction of the stator mesh is needed combined with set proper boundary conditions allows significant reduction in computation time. In order to obtain high symmetry, 10

electrodes (polarized alternately) are assumed to be uniformly distributed on the circumference. Figure 3 shows the resonance frequency and the model shape obtained by meshing 1/10 of the stator, which is equal to 1/2 wavelength of the 5-wavelength mode. The volume is chosen with a total of 2340 mesh elements and total number of degree of freedom is 11000. Using a Sun workstation and an ANSYS program with these conditions the calculation time lasted 360 seconds. The computed resonance frequency of 47.208 kHz was found very close to the measured value of 47.29 kHz.

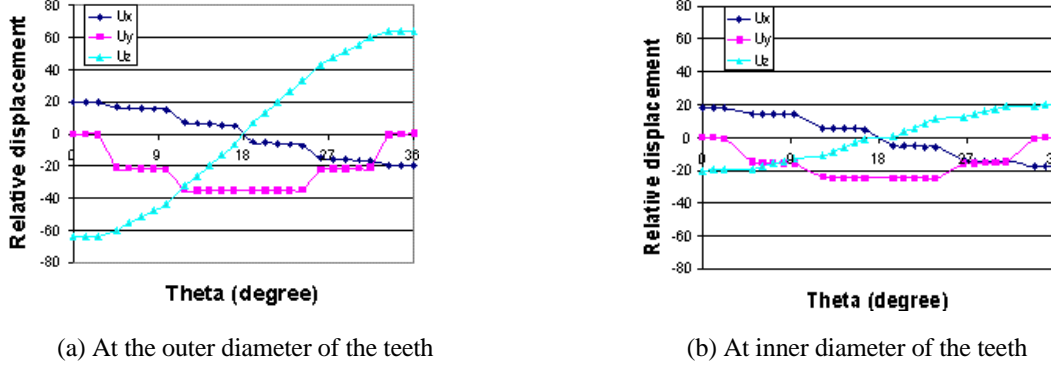


Figure 4: Distribution of the displacements on the top surface of the teeth, U_x is in radial direction, U_y in circumference direction, and U_z is in axis direction.

The 3D model provides detailed displacement distribution of the mode on the tips of the teeth. The tip motion of the traveling wave is obtained by adding two vibration models separated by 1/4 wavelength in space and 90° out of phase in time. As shown in the Figure 4, the radial displacements of the tips are comparable with the circumferential. The results also show that both normal and circumferential displacements at the inner diameter of the teeth are significantly less than those at the outer diameter. The ratio of the normal displacement over the circumferential is greatly changed as well. All these phenomena are important for stator-rotor reaction and motor design.

2.3 The equivalent circuit and electric impedance of the stator

The response of the stator at the frequency around the resonance can be presented by an equivalent circuit. The 3D finite element model was formulated for one terminal case, i.e. all the positively or negatively polarized areas are connected. In this case, the equivalent circuit is presented in Figures 5(a) and (b), where for this circuit there are two resonance frequencies. One is the series resonance F_s , which is equal to the resonance we computed by the 3D finite element model. The other is known as parallel resonance F_p . The F_p is computed in the same way as F_s in the 3D finite element model but without setting V_e to zero. At low frequency, the input impedance is a capacitance C^t given by

$$C^t = C_0 + C_{et} \quad (4)$$

where C_0 and C_{et} are the clumped and motion capacitance in the equivalent circuit of Figure 5(b) respectively.

Generally, the capacitance C^t can also be computed by the finite element model. The three parameters in Figure 5 (b) can be determined using the Electro-mechanical circuit. The stator actually has two electric input terminals; each is connected to partial electrodes. To obtain the equivalent circuit for the partial electrodes, the circuit in Figure 5(a) is redrawn as 5(c) to represent the case of two terminals. When the two terminals are connected in parallel, Figure 5(c) is the same as 5(a).

$$C_{e1} = C_e \left(\frac{n}{m} \right)^2 \quad L_{e1} = L_e \left(\frac{m}{n} \right)^2$$

When the voltage is applied to one terminal and another is shorted, Figure 5(c) becomes 5(d). We have

$$C_1 = C_0 \frac{n}{m}$$

where m is the total number of the electrodes, and n is the number of effectived electrodes.

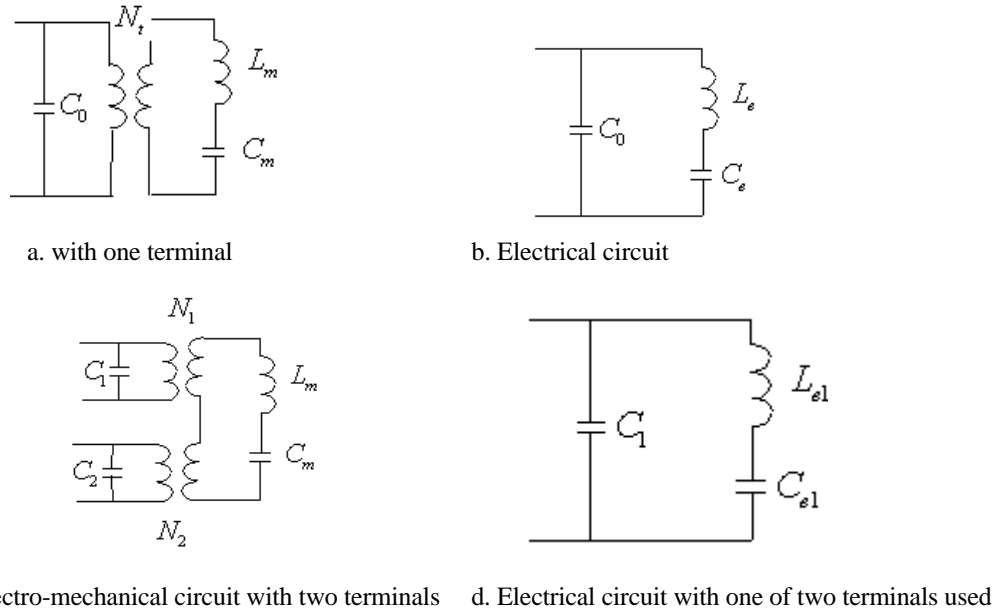


Figure 5: Equivalent circuit for the piezoelectric structure with one or two terminals

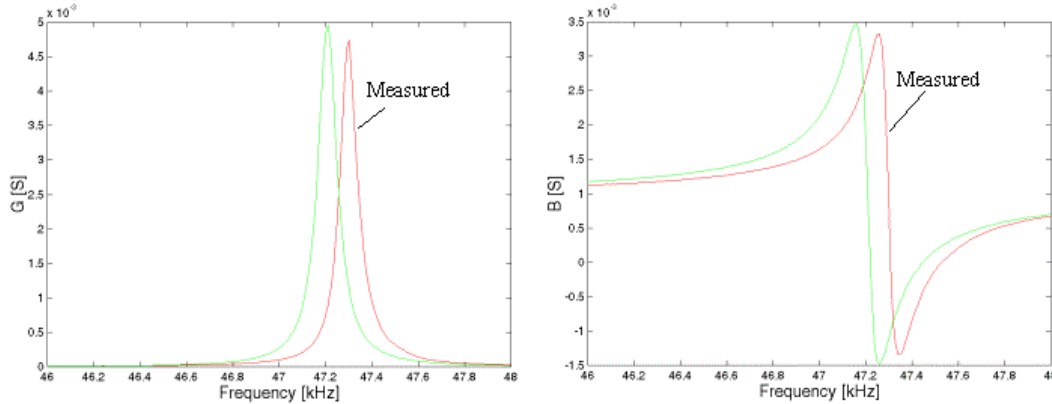


Figure 6: Computed electric impedance versus measured

The input impedance is calculated according to the equivalent circuit after adding a resistor to take in count the mechanical loss. The value of the resistance is determined by the measured Q_m . The result is shown in Figure 6 with the measured impedance. The main difference between the theoretical prediction and the experimental is a frequency shift of 0.1 kHz. This good agreement demonstrates the accuracy of the equivalent circuit. This equivalent circuit is now ready for further model enhancement to include the rotor reacting force and the coupling with the electric driver.

3. CRYOVAC TESTS OF PIEZOELECTRIC MOTORS

The ability of ultrasonic motor to operate at cryogenic temperatures and vacuum is an important characteristics for planetary applications, such as the planet Mars. To establish a baseline for the performance of a USM that was made by JPL/QMI, a commercial motor with a diameter of 1.2-inch was used (Shinsei Model USR30) and was tested at 150°C and 16 mTorr till failure. At the initial phase of the study no efforts were made to deal with the issue of cold start, where the motor is activated after being brought to the cryovac conditions and held to reach steady state before activation. The USR30 motor failed after over 67 hours of operation at the cryovac conditions. To examine the cause of failure, an ultrasonic C-scan nondestructive test was made and the discontinuities were imaged on the computer monitor. As anticipated, the bond between the stator and piezoelectric ring wafer failed. The use of a continuous ring is subjected to thermal stresses that are aggravated by the cyclic mechanical loading of the motor operation leading to fatigue failure of the bond line. JPL in cooperation with QMI replaced the continuous ring with a segmented and reversed piezoelectric drive (SRPD) wafers

allowing to effectively relief the thermal and dynamic stresses at the bonding layer. An SRPD type USM failed after 336 hours total of cryovac test (65 hour at -80°C and 25-mTorr plus 271 hours at -150°C and 16-mTorr). A slower operation was observed after about 210 hours, which may have been the result of a single segment failure. After about 8 hours from the beginning, the SRPD motor had an electric wiring disconnect probably due to fatigue, which was fixed. To determine the robustness of the motor during the cryovac test, it was subjected to 36 stall-torque tests. This test result showed that the use of segmented wafer led to more than 5 times longer lifetime operation at low temperature and vacuum environment. While more motors need to be tested to obtain sufficient statistics however the significant difference of 5 times longer longevity is a very encouraging feasibility demonstration. Investigation of the causes of cold-start failure revealed that the grease in the bearing is freezing. Removal of the grease allowed the operation of the ultrasonic motor down to -150°C . Other issues that were studied include the performance at cyclic temperature environment and vacuum as on Mars.

A temperature cyclic setup was established to allow operation in periods of 2 hours where the temperature is changed from -90°C to 0°C under 7 Torr in our modified cryovac chamber. The choice of temperature and vacuum range was made to simulate Mars environment. The tested ultrasonic motor did not show any significant change in performance and after 231 temperature cycles the experiment was halted. The torque-speed curve, showing the performance before and after thermal cycling, are presented in Figure 7 and the apparent increase in performance is not sufficiently significant to be considered. The loop appearance of the curve is the result of the loading and unloading of the motor and the difference between the two is caused by variations in the motor braking mechanism that is used.

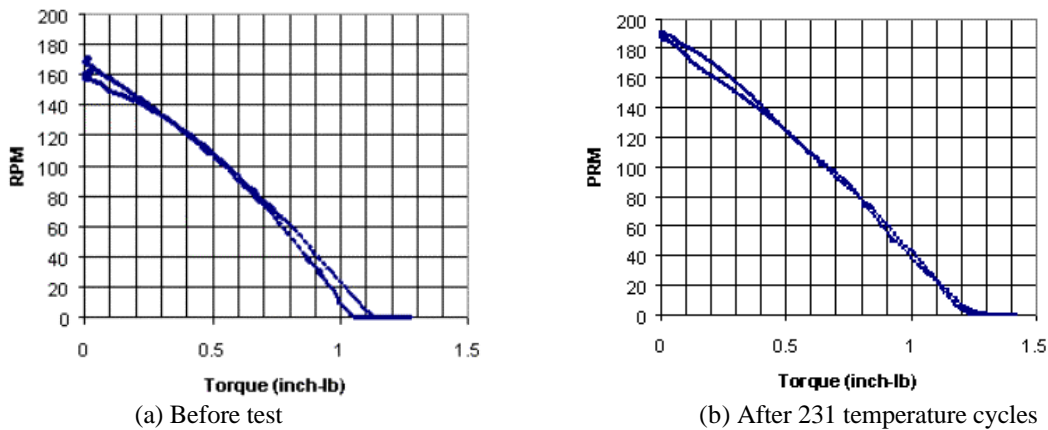


Figure 7: Temperature cyclic test

4. CONCLUSIONS

A 3D finite element model was developed to analyze the spectral response of the stator of ultrasonic motors. The model accounts for the piezoelectric wafers layer, the complex geometrical configuration and construction materials. The modal response and the predicted resonance conditions were corroborated experimentally. Further, in order to couple the 3D finite element analysis with stator-rotor interaction models and electric drivers, an equivalent circuit for the operating mode was reduced. In addition, cryovac tests were made on USMs and showed that the motors can be driven from room temperature down to -150°C and 16-mTorr and still operate for over three hundred hours. The cold start issue that affected the operation of the motors at temperature below -70°C was found to result from the grease in the bearing and its removal eliminated the problem. Further, the motor was exposed to an accelerated simulated Mars a thermal condition for over 200 cycles and no significant change in performance was observed.

ACKNOWLEDGMENT

The results reported in this manuscript were obtained under the Planetary Dexterous Manipulator (PDM) Task, which is managed by Dr. Hari Das. PDM is a NASA Telerobotics task supported by a JPL, Caltech, contract with NASA Headquarters, Code S and Dr. Chuck Weisbin is the JPL Program Manager. The first two authors would like to express their condolences for the passing away of their co-author, Mr. Willem Grandia, on November 12, 1998.

REFERENCES

Allik H., and T.J.R. Hughes, "Finite Element Method for Piezoelectric Vibration," Int. J. Num. Math. Eng., Vol. 2, 1970, pp. 151-157.

- Bar-Cohen Y., X. Bao, and W. Grandia, "Rotary Ultrasonic Motors Actuated By Traveling Flexural Waves," Proceedings of the SPIE International Smart Materials and Structures Conference, SPIE Paper No. 3329-82, San Diego, CA, 1-6 March 1998.
- Flynn A. M., et al "Piezoelectric Micromotors for Microrobots" J. of MEMS, Vol. 1, No. 1, (1992), pp. 44-51.
- Gorman D. G., "Natural Frequencies of Transverse Vibration of Polar Orthotropic Variable Thickness Annular Plates," J. of Sound and Vibrations, Vol. 86 (1), 1983, pp. 47-60.
- Hollerbach M., I. W. Hunter and J. Ballantyne, "A Comparative Analysis of Actuator Technologies for Robotics." In Robotics Review 2, MIT Press, Edited by Khatib, Craig and Lozano-Perez (1991).
- Inaba E., et al, "Piezoelectric Ultrasonic Motor," Proceedings of the IEEE Ultrasonics 1987 Symposium, pp. 747-756, (1987).
- Kagawa K., T. Tsuchiya and T. Kataoka, "Finite Element Simulation of Dynamic Responses of Piezoelectric Actuators," J. of Sound and Vibrations, Vol. 89 (4), 1996, pp. 519-538.
- Wallashek J., "Piezoelectric Motors," J. of Intelligent Materials Systems and Structures, Vol. 6, (Jan. 1995), pp. 71-83.